Drying Technology
Publication details, including instructions for authors and subscription information:
http://www.informaworld.com/smpp/title~content=t713597247

Fractal Characteristics and Scaling of the Drying Front in Porous Media: A Pore Network Study

A. G. Yiotis[a]; I. N. Tsimpanogiannis[a]; A. K. Stubos[a]
[a] Environmental Research Laboratory, National Center for Scientific Research "Demokritos", Aghia Paraskevi, Greece

Online publication date: 05 August 2010

To cite this Article Yiotis, A. G. , Tsimpanogiannis, I. N. and Stubos, A. K.(2010) 'Fractal Characteristics and Scaling of the Drying Front in Porous Media: A Pore Network Study', Drying Technology, 28: 8, 981 — 990
To link to this Article: DOI: 10.1080/07373937.2010.497087
URL: http://dx.doi.org/10.1080/07373937.2010.497087

Drying Technology, 28: 981–990, 2010

ISSN: 0737-3937 print/1532-2300 online
DOI: 10.1080/07373937.2010.497087

Taylor & Francis
Taylor & Francis Group

Fractal Characteristics and Scaling of the Drying Front in Porous Media: A Pore Network Study

A. G. Yiotis, I. N. Tsimpanogiannis, and A. K. Stubos
Environmental Research Laboratory, National Center for Scientific Research "Demokritos", Aghia Paraskevi, Greece

We perform two-dimensional pore network simulations of isothermal drying in order to provide better insight on the structure of the drying patterns, particularly in the frontal region, both in the presence and absence of gravity forces. Our numerical results for the fractal dimension of the invading gaseous phase ($D_p = 1.88 \pm 0.03$) and the drying front perimeter ($D_e = 1.34 \pm 0.06$) in the absence of gravity are in very good agreement with reported experimental and theoretical values. The scaling of the drying front width, σ_f, in the presence of a front-stabilizing gravity gradient is also examined and it is found to scale with the Bond number (ratio of gravity to capillary forces) as $\sigma_f \propto |B|^{-0.58}$. The width of the finger, ξ, that develops by a front-destabilizing gravity gradient is found to scale as $\xi \propto |B|^{-0.57}$. We also report the effects of gravity forces on the drying rates and their scaling.

Keywords Drying; Fractal; Invasion percolation; Pore network; Porous medium; Scaling

INTRODUCTION

Drying of porous media is a liquid to gas phase change process that has a wide range of industrial applications. It is involved in the production process of a variety of commercial products such as paper, food, pharmaceuticals, textile, wood, ceramics, granular and building materials, etc. In a different but related context, drying is also involved in distillation and vaporization processes associated with soil remediation,[1] as well as in the recovery of volatile oil components from fractured reservoirs by gas injection (Lenormand et al.[2] and Tsimpanogiannis et al.[3] and references therein).

The complicated nature of drying in porous media, combined with the wide range of applications related to this liquid to gas phase change process, has resulted in a plethora of studies that have appeared in literature. Van Brakel[4] has provided extensive insight into the drying process by analyzing experimental results and modeling studies. Traditionally, the process is approached from a phenomenological point of view. Luikov[5] and Whitaker[6,7] offered a good account of such methods in their extensive reviews. Under this approach, the porous medium is replaced by a hypothetical effective continuum, in which the detailed physics at the pore level are lumped into averaged quantities (see the comprehensive numerical simulator by Perre and Turner[8]). Equivalent-continuum partial differential equations are used to describe the temporal and spatial evolution of volume-averaged quantities (e.g., temperature, moisture content, etc.). Closure to the problem is provided using empirical parameters, which often require fitting to some kind of experimental data. Alternatively, such parameters could be evaluated using pore network models.

Pore network studies represent an improvement in modeling that has been achieved in recent years. They have been primarily used to study two-phase or multiphase displacement processes in porous media. Blunt et al.[9] presented a detailed review. Lately they have been used to study processes in porous media where heat,[10] mass transfer,[11–14] and reaction[15–17] are important. Pore networks studies that examine drying/evaporation in porous media are discussed in the remaining of the section.

Following the pore network description one can represent the porous medium as an ensemble of pores and throats of different geometries and sizes that can take values from appropriate distributions. In this approach emphasis is placed on incorporating into the pore network models the detailed physics occurring at the single-pore level. Such studies can contribute to the fundamental understanding of how phenomena occurring at the pore level can influence processes at the larger (effective continuum) scale. Note, however, that the detailed description that is achieved with pore network modeling requires significantly more computational power, therefore limiting the size of the problems that can be considered.

Drying is a two-phase flow process that involves many pore-scale mechanisms that affect the macroscopic behavior of the process. These include the motion of individual gas–liquid menisci residing in the pore space under the

Correspondence: A. G. Yiotis, Environmental Research Laboratory, National Center for Scientific Research "Demokritos", Aghia Paraskevi 15310, Greece; E-mail: yiotis@ipta.demokritos.gr

combined effect of capillary, viscous and buoyancy forces, the mass and heat transfer by diffusion and convection in the gas and liquid phase, viscous flow in both phases, liquid flow through connected films, and liquid remaining at the corners of noncircular pores. All these mechanisms need to be accounted for at the pore scale. A number of pore network studies of varying degree of complexity have been presented during recent years that attempted to incorporate various aspects of the drying process.[18–42] More physical details of the drying process incorporated in a pore network simulator result in obtaining more realistic simulations but at the cost of higher computational demands.

During the drying process, a single- or multicomponent liquid phase that initially saturates partially or completely the porous medium gradually evaporates and is removed from the porous structure. The drained pore space is subsequently invaded by air. This sequence of events resembles those observed during immiscible displacement (ID) inside porous media. During an ID process (e.g., drainage) the porous medium is initially saturated with a wetting phase (defending phase). The wetting phase is displaced by the injection of a nonwetting phase (invading phase). For the case of drying considered in this study, the network is initially completely saturated with liquid. Due to evaporation, air invades the system. Technically, however, the gas phase does not displace the liquid but invades the "empty space" created from the evaporation of the liquid phase.

Figure 1 shows a schematic of the immiscible displacement and the evaporation processes. Depicted also are some of the differences between the two processes. In particular, at the ID the invading phase enters from one side and the displaced defending phase exits from the opposite open end. On the other hand, during the evaporation process the invading phase (air) and the receding fluid (in particular the vapors of the liquid phase) counterdiffuse toward the same open side. During an ID, as a result of the incompressibility of the defending wetting phase, smaller clusters can be completely surrounded by the invading phase and become disconnected ("trapped") from the main defending phase cluster. Such clusters do not participate any further in the invasion process. For the case of drying, however, such trapped clusters continue to evaporate until they are completely eroded. Note, here, that the drying process is driven by diffusion in the gas phase.

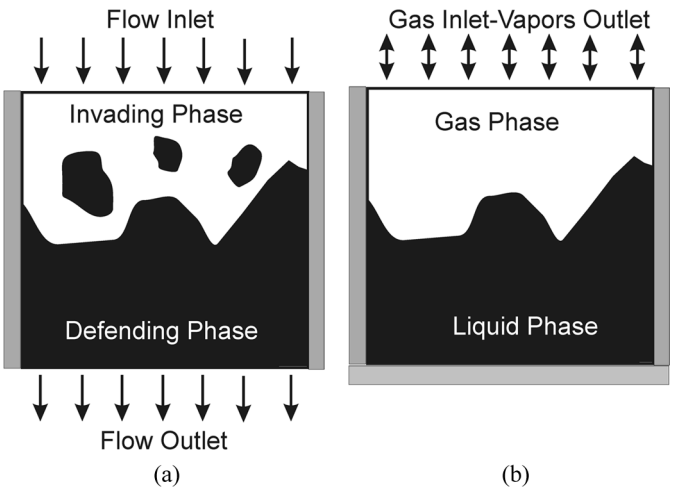

FIG. 1. Schematic of two-phase flow processes: (a) immiscible displacement and (b) drying/evaporation.

Shaw[43] was among the first to consider the drying process as a modified form of immiscible displacement. He conducted drying experiments in Hele-Shaw cells placed horizontally with dimensions 2.5 cm × 4.0 cm and thickness 15–20 μm, packed with silica spheres of size 0.5 μm, and analyzed the obtained images of the drying experiments in order to obtain the scaling of the drying front. It is known that when a less viscous nonwetting fluid (air) displaces a more viscous wetting fluid (water), unstable displacement finger-type fronts are expected. Shaw attributed the drying front stability in the removal of the liquid phase from the pore structure to the counter-flow of liquid films in the displacing fluid. The important role played by the viscous forces on the stabilization of the drying front was discussed in additional detail by Tsimpanogiannis et al.[44] and Prat and Bouleux.[23]

In the current study, we perform 2D pore network simulations of isothermal drying in order to better understand the structure of the drying patterns, particularly in the frontal region. We consider the simpler case where no viscous effects are taken into consideration during the pore network simulations. However, the effects of gravity forces are considered. We report results for the fractal dimension of the invading phase and the drying front perimeter in the absence of gravity. We also examine the scaling of the drying front width in the presence of a front-stabilizing gravity gradient, as well as the width of the finger that develops by a front-destabilizing gravity gradient. We also report on the effects of gravity forces on the drying rates and their scaling.

METHODOLOGY

The model discussed in this study is based on the work of Prat,[19,20] Laurindo and Prat,[21,22] and Prat and Bouleux.[23] It is applied, however, to further analyze the fractal characteristics and the scaling of the drying front, the phase distribution patterns, and the drying rates of larger pore networks under the influence of gravity.

The porous medium is represented by a 2D regular square network of spherical pores that are connected through cylindrical throats. The radius of the pores is taken constant and equal to 500 μm. The throat radius follows a random distribution with a range 50–100 μm. The lattice

length l (pore center to pore center distance) is equal to 2 mm. As a result of the considered values for the pore/throat radius, the pores provide the volumetric storage and the throats provide the resistance to flow and mass transfer. The following assumptions are made in our simulations:

- The fluids are stored in the pores only, because the volume of the throats is significantly smaller.
- The capillary pressure is significant in the throats and negligible within the pores.

For the aforementioned network we can identify the following three types of pores (see also the discussion by Tsimpanogiannis et al.[44] and Yiotis et al.[25]): those pores that are fully occupied by gas (belonging to the gas phase and denoted by G), those pores that are fully occupied by liquid (belonging to the liquid phase and denoted by L), and those pores located at the gas–liquid interface (in which a meniscus resides, denoted by I). The latter can be further subdivided in completely empty (CE) and partly empty (PE) pores.

When the gas–liquid interface is located inside an interface throat, it remains temporarily pinned due to capillary forces; however, evaporation continues to occur. The difference in pressure due to capillary forces is

$$P_c = P_{nw} - P_w = \frac{2\gamma}{r} \tag{1}$$

where P_{nw} and P_w correspond to the pressures of the nonwetting (nw) and wetting (w) phases, respectively; r is the radius of the throat; and γ is the interfacial tension and we assumed a zero contact angle. When the gravity forces are important, the capillary pressure will vary with the elevation h of the interface as follows:

$$P_c = \frac{2\gamma}{r} + g_x h \Delta\rho \tag{2}$$

where g_x is the component of gravity in the direction of displacement and $\Delta\rho = \rho_w - \rho_{nw}$.

As a result of the continuous evaporation of the liquid phase, the gas–liquid interface recedes inside the pore network and eventually isolated liquid clusters that are disconnected from the main liquid phase are formed. These clusters are surrounded by the invading continuous gaseous phase. Let us consider an isolated liquid cluster where the gas–liquid interface is pinned due to capillary forces at the throats of the perimeter. Evaporation from that cluster continues and eventually one of the throats (and the adjacent liquid pore) belonging to the external perimeter of the cluster is invaded (the one with the minimum capillary threshold). This process is continued until the liquid cluster is completely evaporated.

The evaporation flux, F_{ij} ($mass/time \times area$), of the liquid from the I pores at the perimeter of the liquid clusters toward the G pores is

$$F_{ij} = D\left(\frac{C_i - C_j}{l}\right) \tag{3}$$

where D is the diffusion coefficient; C_i and C_j are the vapor concentration at the I pore (taken equal to the equilibrium concentration C_e) and G pore, respectively; and l is the distance between the centers of the two pores. The vapors are transferred by diffusion to the open end of the network. The mass flow rate by diffusion through a throat with radius r_{ij} and cross-sectional area A_{ij} that connects two adjacent G pores is

$$Q_{ij} = A_{ij}F_{ij} = \pi r_{ij}^2 D\left(\frac{C_i - C_j}{l}\right) \tag{4}$$

At steady-state the mass balance inside every pore in the gas phase is given by

$$\sum_j Q_{ij} = \sum_j \pi r_{ij}^2 D\left(\frac{C_i - C_j}{l}\right) = 0 \tag{5}$$

The gas phase saturation inside an I pore (of type PE) is calculated through the following mass balance:

$$S_i^{t+1} = S_i^t + \frac{\Delta t}{\rho_l V_l} \cdot \sum_j Q_{ij} \tag{6}$$

where S_i^{t+1} is the gas saturation inside the pore at the next time step $(t+1)$, S_i^t is the gas saturation inside the pore at the current time step (t), and Δt is the time step during which we assume constant rate Q. Equations (3)–(6) are used to calculate the recovery rate during the drying process.

NUMERICAL RESULTS AND DISCUSSION

A large number of drying simulations were performed using 2D pore networks with dimensions $L \times L$, where L denotes the number of pores in each dimension. A similar set of simulations was performed for the case of invasion percolation with trapping (IPT) to model drainage processes. The networks had three sides impermeable and one side open to flow and mass transfer. Isothermal conditions were assumed. The largest pore network used was with $L = 600$ and required approximately 58 h for completion of the simulation of a single realization when using an Intel P4 2.53-GHz personal computer (PC). The respective time dropped to about 30 min for a 300×300 pore network. Each simulation was continued until the invading gas phase reaches the side opposite to open one

(breakthrough point, BT). At that moment we have the formation of a sample-spanning cluster of the invading phase (gas). That moment also corresponds to the critical point of the ordinary percolation (OP) where we have the creation of the infinite (percolating) cluster.[45]

In this study we considered hexane as the liquid that initially completely saturated the pore network. The following values for the parameters were used during the numerical simulations: interfacial tension $\gamma = 19 \times 10^{-3}\,\mathrm{N/m}$, liquid-phase density $\rho_l = 650\,\mathrm{kg/m^3}$, gas-phase density $\rho_g = 4.4\,\mathrm{kg/m^3}$, equilibrium concentration $C_e = 0.266\,\mathrm{kg/m^3}$, and binary diffusion coefficient of hexane into air $D = 6.38 \times 10^{-6}\,\mathrm{m^2/s}$.

EFFECT OF CAPILLARY FORCES (WITH $g = 0$)

When the flow of the invading phase is very slow and in the absence of gravity, capillary forces dominate over viscous forces at the liquid–gas interface. In this case, the movement of the interface, as the liquid evaporates, is determined by the size of throat radii. Among all throats belonging to the invasion front, the one with the minimum capillary threshold (i.e., larger throat radius) will be invaded. Because the size of the throats is distributed randomly, the probability of throat invasion is random in space as well. The sequence of pore invasion can be modeled with invasion percolation (IP).[46] As a result, the invading phase will acquire a self-similar fractal pattern, which eventually approaches that of the percolation cluster.[47] Prat[20] demonstrated numerically that the invasion front resulting from evaporation and drainage was the same fractal object. Figure 2 shows three typical snapshots of phase distribution patterns obtained from 150×150 pore network simulations of drying in the absence of gravity forces.

Fractal Dimension of Drained Space

According to percolation theory, the mass, M, of the percolating gaseous cluster, which is proportional to the number (N) of invaded pores, is known to scale with the correlation length ξ_p (i.e., the characteristic size of the cluster) as follows[48]:

$$M(\xi_p) \propto \xi_p^{D_p} \tag{7}$$

where D_p is the fractal dimension of the percolation cluster. The theoretical value for 2D from ordinary percolation (OP) is $D_p = 91/48 = 1.89$,[49] whereas the value from numerical simulations for invasion percolation without trapping (IPWT; i.e., drying) is $D_p = 1.89$ and for IPT (i.e., drainage) is $D_p = 1.82$.[46] For the case of IPT, the incompressibility of the defending phase, which results in the trapping of the defending phase, renders large areas of the network to be unavailable for invasion. Therefore, the number available for invasion pores is less, and the liquid recovery at the critical point is lower when trapping is taken into consideration.

In finite systems at the "critical" point, that is, when the gas phase reaches the side opposite to the open one, the correlation length equals the size of the system $\xi_p = L$. Therefore, Eq. (7) becomes

$$M(L) \propto L^{D_p} \tag{8}$$

By varying the size L of the system and counting the number of invaded pores at BT, we can obtain the fractal dimension D_p of the percolating cluster. We performed such an analysis for the invading phase that resulted from the drying simulations. Figure 3 shows a log-log plot of the number of gas-invaded pores (drained pores) as a function of the lattice size L for several hundreds of realizations. These results correspond to a series of numerical simulations with several hundred random pore networks of sizes ranging from $L = 30$ to $L = 600$. The slope of the curve is equal to the fractal dimension D_p.

The mass of the invading phase was measured by counting the number of pores occupied by the invading phase (air) at the critical point for various sizes of the pore network L. Note that for the case of drying simulations we ignored the effect of the gradient in the concentration during the calculation of the mass fractal dimension of the invading phase. Essentially we considered that all *PE* pores empty with the same rate without considering their distance

FIG. 2. Phase distribution during drying for the case $g = 0\,\mathrm{cm/s^2}$ inside a 150×150 pore network. Liquid phase is shown in black and gas phase in white. Open end at the top side.

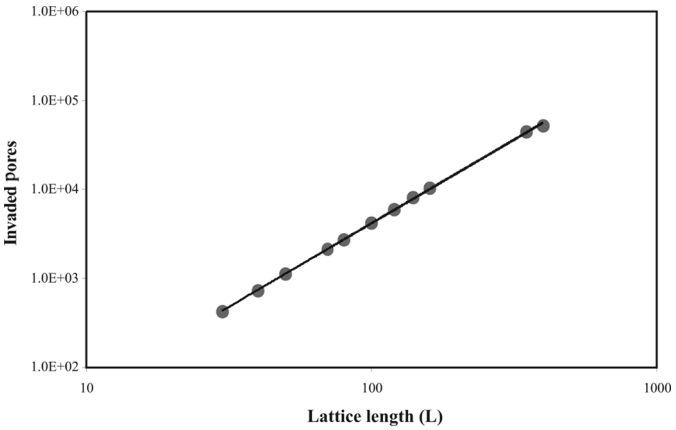

FIG. 3. Log-log plot of the number of gas-invaded pores (dried pores) as a function of the lattice length L (in lattice units).

from the open end of the network where $C = 0$. Under this assumption we calculated that the fractal dimension of the invading phase is $D_p = 1.88 \pm 0.03$. This value is in excellent agreement with the experimental value for drying in Hele-Shaw cells packed with silica spheres, $D_p = 1.89 \pm 0.03$, 0.03, reported by Shaw.[43] The obtained value from our drying numerical simulations is also in excellent agreement with the theoretical value $D_p = 1.89$ resulting from OP,[49] as well as with numerical results from invasion percolation without trapping $D = 1.89$.[46] Recall at this point that during the drying process the liquid clusters left behind as the drying front advances inside the porous medium evaporate completely. Therefore, the drying process produces invasion patterns that are closer to IPWT than to IPT.

The saturation of the nonwetting (invading) phase is equal to $S_{nw} = N/L^d$, where N is the number of the invaded pores and d is the dimensionality of the pore network. The saturation scales as follows[46]:

$$S_{nw}(L) \propto L^{-\alpha} \tag{9}$$

where the exponent α is related to the fractal dimension D_p and the space dimension d by

$$\alpha = d - D_p \tag{10}$$

From our numerical simulations we calculated that $\alpha = 0.12 \pm 0.01$ in good agreement with the theoretical value ($\alpha = 0.11$).

Fractal Dimension of the Drying Front

Of interest also is the external perimeter of the percolation cluster. For the case of drying this corresponds to the drying front. Essentially it includes all the liquid-occupied pores at the perimeter that have a gas-occupied pore as a next-nearest neighbor.

The fractal dimension of the interface for the drying process was calculated using the "box-counting" method.[47,50] The fractal set is completely covered by nonoverlapping boxes of Euclidean size δ. The number $N(\delta)$ of such boxes required is plotted and the following relation is used in the limit $\delta \to 0$:

$$N(\delta) \propto \delta^{-D_e} \tag{11}$$

Figure 4 shows the double-logarithmic plot of the number of gas-invaded pores at the front as a function of the box size δ. Results from 10 realizations of 200×200 networks were utilized. The value for the fractal dimension of the interface for the drying process was calculated to be $D_e = 1.34 \pm 0.06$. This value is in good agreement with the experimental value for the fractal dimension of the external perimeter, $D_e = 1.38 \pm 0.02$, of the drying front reported by Shaw.[43]

Our numerical results are also in good agreement with reported values for drainage in the literature. In particular, Birovljev et al.[51] reported the following computational ($D_e = 1.39 \pm 0.02$) and experimental ($D_e = 1.34 \pm 0.04$) values for drainage. Grossman and Aharony[52] reported the value $D_e = 1.37 \pm 0.03$ from computer simulations of site percolation clusters for the case when considering nearest-neighbor connectivity.

Effect of Gravity Forces

If we consider the gravity forces to be part of the drying process ($g \neq 0$), then an IP will not develop over the entire region of the displacement. Instead, the displacement follows the features of invasion percolation in a gradient (IPG).[51,53–56] The Bond number, B, which is the ratio of gravity to capillary forces, is a measure of the competition between the gravity and capillary forces during the displacement. The Bond number is given by

$$B = \frac{g_x r_m^2 \Delta\rho}{\gamma} \text{ or } B = \frac{g_x k \Delta\rho}{\gamma} \tag{12}$$

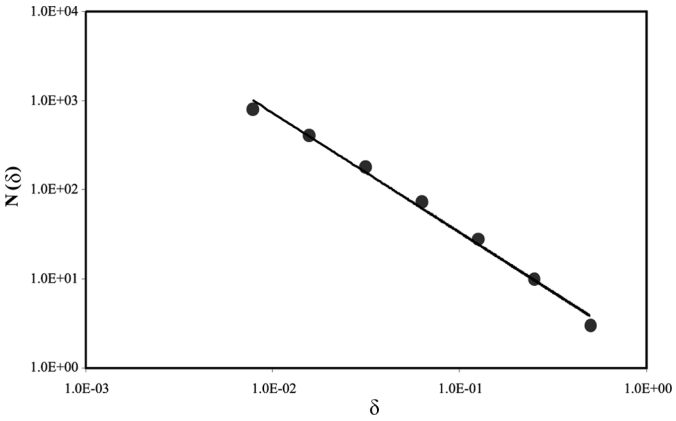

FIG. 4. Log-log plot of the number of gas-invaded pores at the front as a function of the box size δ (in lattice units).

where k is the permeability of the pore network and $k \propto r_m^2$ (r_m is the mean pore size). We can distinguish two cases:

1. When $B > 0$ (i.e., downward displacement of a heavier fluid by a lighter fluid), the two phases are separated by a front of finite width, σ_f, which scales with the Bond number as

$$\sigma_f \propto B^{-\nu/(\nu+1)} \tag{13}$$

where ν is the correlation length exponent of percolation, with values $\nu = 4/3$ in 2D and $\nu = 0.88$ in 3D.[45] Therefore, the theoretical predictions for the exponent $-\nu/(\nu+1)$ are equal to -0.57 for 2D and -0.47 for 3D. Figure 5a shows a schematic of the front width σ_f. As a result of the self-affinity of the front it is useful to define the drying mean-front position, x_f, as follows for the case of 2D (see also the detailed discussion by Gouyet et al.[57] and Gouyet and Rosso[58] for the case of 3D diffusion fronts).

$$x_f = \frac{\int_0^\infty x \cdot p_f(x)dx}{\int_0^\infty p_f(x)dx} \tag{14}$$

where $p_f(x)$ is the probability to find a pore of the interface at x. The mean-front position and the width of the front are related through

$$\sigma_f^2 = \frac{\int_0^\infty (x - x_f)^2 \cdot p_f(x)dx}{\int_0^\infty p_f(x)dx} \tag{15}$$

2. When $B < 0$ (i.e., upward displacement of a heavier fluid by a lighter fluid), the invasion process is dominated by the growth of a single invading finger (branch), the local characteristics of which are still controlled by percolation. The finger can be described as a chain of fractal blobs that have a characteristic length ξ. Figure 5b shows a schematic of the front width ξ. The mean width of the finger is proportional to the characteristic length and scales as

$$\xi \propto |B|^{-\nu/(\nu+1)} \tag{16}$$

Namely, it follows the same scaling as the mean width of the front for the stabilizing case. This regime has been studied in detail by Frette et al.[59] and Meakin et al.[60,61]

Stabilizing Gradient Pore Network Results ($B > 0$)

In the current study we consider that the gravity g is parallel to the invasion direction and constant in the entire network. For the case where the gravity vector has the same direction with the velocity vector of the drying front (i.e., $B > 0$), the gravity forces stabilize the interface and tend to limit the front width σ_f (see Fig. 5a). Figure 6 shows the evolution of the phase distributions during drying for two values of the parameter B. As can be seen, the width of the front of the gas–liquid interface is a function of B or equivalently g. The higher the value of g, the stronger are the hydrostatic forces that act on the interface and the smaller the width of the front σ_f.

In order to study the dependency of the width of the drying front on the value of g, a series of numerical simulations was conducted and we measured the front width using Eq. (15). For values of $g \geq 10\,\mathrm{cm/s^2}$ we used 100 realizations of 200×200 pore networks, whereas for values

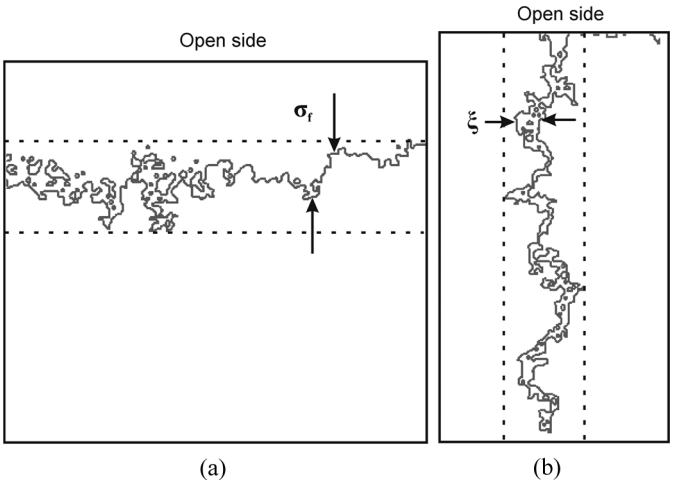

FIG. 5. Schematic of the drying front: (a) front width for the case of the stabilizing gradient and (b) finger mean width for the case of the destabilizing gradient.

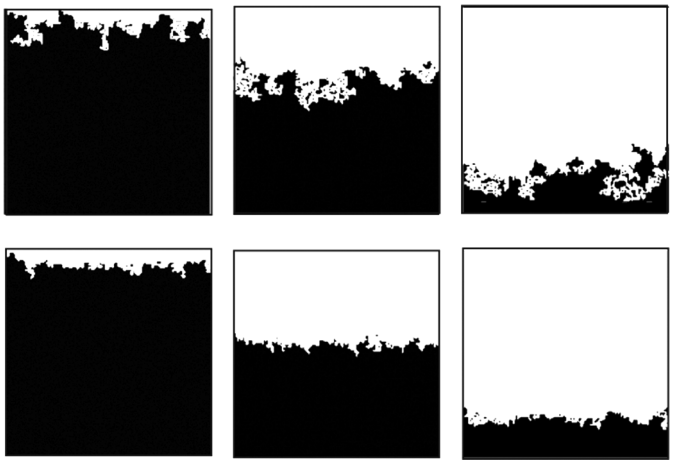

FIG. 6. Evolution of phase distribution during drying under stabilizing gradient ($B > 0$). $g = 10\,\mathrm{cm/s^2}$ (top panel), and $g = 30\,\mathrm{cm/s^2}$ (bottom panel). Liquid phase is shown in black and gas phase in white.

of $g < 10\,\mathrm{cm/s^2}$ we used 10 realizations of 600×600 pore networks. The front width was measured at the critical point (invading gas phase reaching the opposite end of the pore network).

Figure 7 shows the averaged values of the front width as a function of g. According to the results from our numerical calculations the width of the front as a function of the gravity force is given by

$$\sigma_f \propto g^{-0.58} \Rightarrow \sigma_f \propto B^{-0.58} \tag{17}$$

The obtained value of the exponent -0.58 ± 0.04 for 2D is in very good agreement with the theoretical prediction, -0.57, of Eq. (13). Prat and Bouleux[23] performed drying simulations in 400×400 pore networks (six realizations) and obtained the value of -0.5738 ± 0.0017.

Similar values were reported from experimental and numerical simulations for drainage in 2D pore networks.[51,53,62]

Destabilizing Gradient Pore Network Results ($B < 0$)

In the case where the gravity vector has the opposite direction of the velocity vector of the receding drying front (i.e., $B < 0$), the gravity forces destabilize the interface and tend to increase the front width σ_f. Figure 8 shows two snapshots of the evolution of the phase distributions during drying for a negative value of the parameter B. We observe that we have the formation of a dominant branch (finger-like structure) that increases continuously in length until it finally reaches the opposite end (critical point).

The width, ξ, of the finger (see Fig. 5b) is almost constant along its length. By changing the value of g (or B) we observe that the average width of the invading finger changes as well. This is clearly demonstrated in Fig. 9,

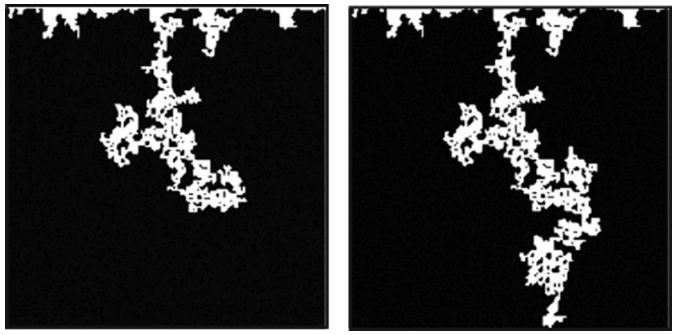

FIG. 8. Evolution of phase distribution during drying under destabilizing gradient ($B < 0$) in 200×200 pore networks ($g = -20\,\mathrm{cm/s^2}$). Liquid phase is shown in black and gas phase in white.

where the percolating gas phase is depicted for three different values of g (i.e., -2, -10, and $-70\,\mathrm{cm/s^2}$).

We apply Eq. (15) in the direction perpendicular to the flow (parallel to the open end of the pore network) and measure the width of the invading finger for various values of g. For each value of g we performed 10 realizations in 300×300 pore networks and the average values of the finger widths are shown in Fig. 10 as a function of $|g|$. To reduce the effect of the inlet and outlet of the network we ignored the finger width that was near the inlet/outlet (within 10% of the network length).

According to the results from our numerical simulations, the width of the invading finger as a function of the gravity force is given through

$$\xi \propto |g|^{-0.57} \Rightarrow \xi \propto |B|^{-0.57} \tag{18}$$

where the finger width ξ is calculated using Eq. (15).

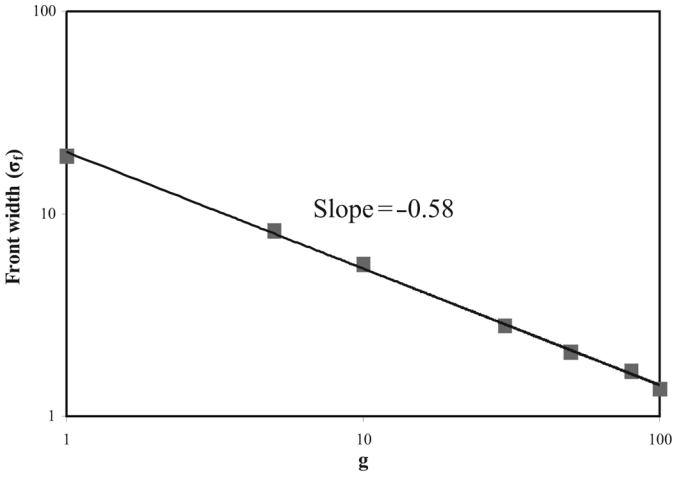

FIG. 7. Front width, σ_f, (in lattice units) as a function of gravity for the drying process under stabilizing gradient. Squares denote the average values obtained from the pore network simulations.

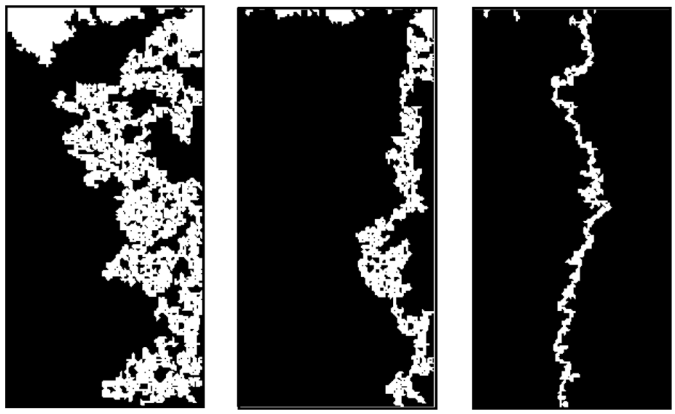

FIG. 9. Phase distribution during drying under destabilizing gradient ($B < 0$) in 100×200 pore networks. The effect of gravity forces on branch width: $g = -2\,\mathrm{cm/s^2}$ (left panel), $g = -10\,\mathrm{cm/s^2}$ (center panel), and $g = -70\,\mathrm{cm/s^2}$ (right panel). Liquid phase is shown in black and gas phase in white.

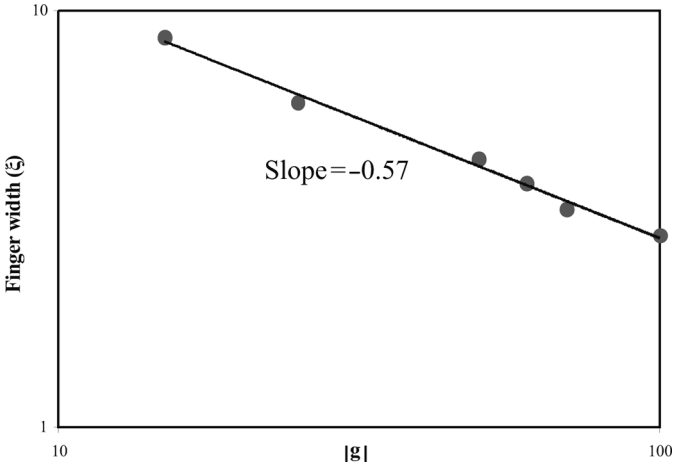

FIG. 10. Log-log plot of the finger mean-width, ξ, (in lattice units) as a function of gravity, $|g|$, for the drying process under destabilizing gradient. Circles denote the average values obtained from the pore network simulations.

The obtained value of the exponent -0.57 ± 0.05 is in very good agreement with the theoretical prediction, -0.57, of Eq. (16). It is also in very good agreement with experimental and numerical results from the literature for the case of drainage in 2D pore networks.[53,60,61]

Effect of Gravity on the Drying Rate

Assuming that the gas–liquid interface (drying front) recedes with an average velocity u_f and the mean front position is x_f, as defined through Eq. (14). Concentration and pressure fields are coupled at the interface by mass balance.[44] Therefore, due to the boundary conditions of the drying process the following scaling holds for the average velocity

$$u_f \propto \frac{D \cdot C_e}{x_f} \tag{19}$$

where D is the diffusion coefficient and C_e is the equilibrium concentration.

The average velocity of the front can also be defined through the mean front position

$$u_f \equiv \dot{x}_f = \frac{dx_f}{dt} \tag{20}$$

By combining Eqs. (19) and (20) we obtain

$$\frac{dx_f}{dt} \propto \frac{1}{x_f} \tag{21}$$

After integration of the above equation we can obtain that the mean front position of the interface is proportional to the square root of the drying time

$$x_f \propto \sqrt{t} \tag{22}$$

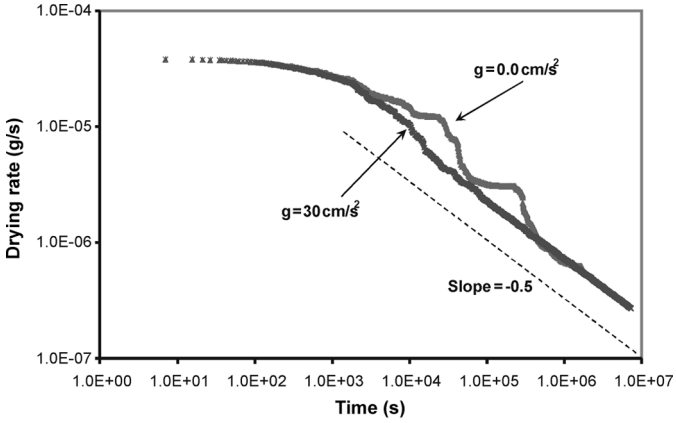

FIG. 11. Drying rates as a function of time for two cases of g. The dashed line shows the theoretical slope equal to -0.50.

and therefore the velocity of the front and the drying rate are inversely proportional to the square root of the drying time

$$u_f \propto t^{-1/2} \text{ and } \dot{m} \equiv Q \propto t^{-1/2} \tag{23}$$

Figure 11 shows in a log-log plot the drying rate as a function of time for two cases of g: A case were the gravity forces are not present ($g = 0\,\mathrm{cm/s^2}$) and a case with $B > 0$ ($g = 30\,\mathrm{cm/s^2}$), for which case the interface recedes almost without perturbations (piston-like).

We observe that during the initial stages of the drying process when the interface is very close to the open end of the pore network, the drying rate remains almost constant for a long period of time (constant rate period, CRP). Yiotis et al.[25] demonstrated using 2D numerical simulations that CRP lasts as long as the liquid phase remains in contact with the open end of the pore network. A more detailed

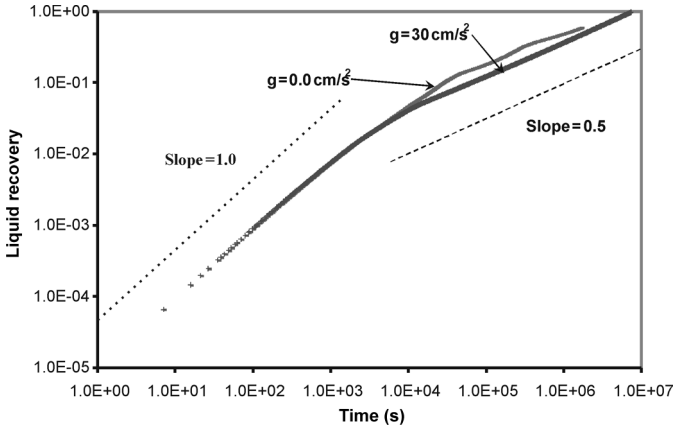

FIG. 12. Drying curves for two cases of g. The dotted line shows the theoretical slope for early times equal to 1.0. The dashed line shows the theoretical for later times slope equal to 0.50.

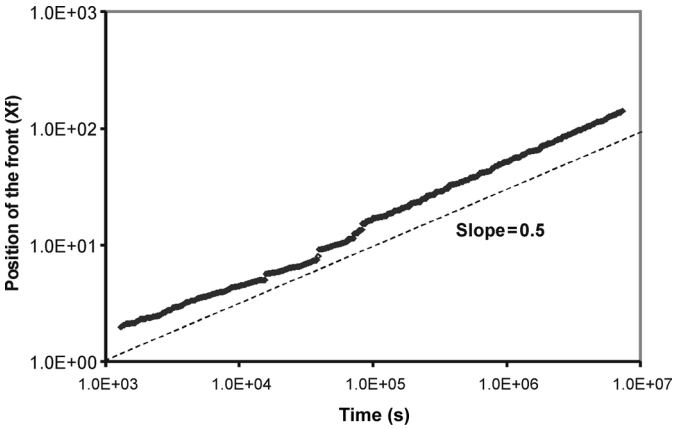

FIG. 13. Mean front position (in lattice units) as a function of time for $B > 0$. The dashed line shows the theoretical slope equal to 0.50.

discussion based on 3D pore network simulations about CRP and other characteristic periods that develop during drying in porous media was presented in Yiotis et al.[34] and will not be further elaborated in this study.

At later times the drying rate becomes inversely proportional to the square root of the drying time, as Eq. (23) dictates. This becomes obvious for the case of large values of B (the interface recedes without significant fluctuations). For the case of $B = 0$ this is not that obvious due to the existence of trapped liquid clusters that become disconnected from the main liquid phase. Figure 12 shows the drying curves for the aforementioned two cases expressed as the recovered liquid saturation, S_l, as a function of time. At early times the liquid recovery is directly proportional to the elapsed time $S_l \propto t$, as shown by Chapuis and Prat[63] in the case where the continuous liquid phase is contact with the open side of the network, either directly (in this work) or through liquid films as in the case of Chapuis and Prat.[63] At later times, when the continuous liquid phase loses contact with the open side, the recovered liquid saturation scales as $S_l \propto t^{0.5}$. As shown in the figure, theoretical prediction and numerical simulations are in good agreement.

Figure 13 depicts the mean front position of the interface as a function of time for the case of $B > 0$. We observe that the mean front position of the interface is proportional to the square root of time as predicted by Eq. (22). The numerical simulations result in a slope equal to 0.51, which is in very good agreement with the theoretical value of 0.50.

CONCLUSIONS

We performed a series of 2D pore network simulations of isothermal drying in order to provide a better understanding of the structure of the drying patterns, particularly in the frontal region in the presence of gravity. The pore network simulator used in this study was based on concepts from invasion percolation in porous media that is driven by mass transfer. Our numerical results for the fractal dimension of the invading phase ($D_p = 1.88 \pm 0.03$) and the drying front perimeter ($D_e = 1.34 \pm 0.06$) in the absence of gravity were found to be in very good agreement with reported experimental and theoretical values.

In the case of a gravity stabilized front, that is, when $B > 0$, the drying front width, σ_f, in the presence of a stabilizing gravity gradient is found to scale with the Bond number as $\sigma_f \propto |B|^{-0.58}$, consistent with theoretical predictions and reported numerical simulations and experiments. In the opposite case of a gravity-destabilized front, the width of the finger, ξ is found to scale as $\xi \propto |B|^{-0.57}$, in excellent agreement as well. We also reported the effects of gravity forces on the drying rates and their scaling.

REFERENCES

1. Ho, C.K.; Udell, K.S. Mass transfer limited drying of porous media containing an immobile binary liquid mixture. International Journal of Heat and Mass Transfer **1995**, *38*, 339–350.
2. Lenormand, R.; Le Romancer, J.F.; Le Gallo, Y.; Bourbiaux, B. *Modeling the Diffusion Flux between Matrix and Fissure in Fissured Reservoir*; SPE paper 49007. Presented at the SPE Annual Technical Conference and Exhibition, 27–30 September 1998, New Orleans, Louisiana.
3. Tsimpanogiannis, I.N.; Stubos, A.K.; Yortsos, Y.C. Evaporation of a stagnant liquid. Industrial Engineering Chemistry Research **2000**, *39*, 1505–1513.
4. Van Brakel, J. Mass Transfer in convective drying. Advances in Drying **1980**, *1*, 212–267.
5. Luikov, A.V. *Heat and Mass Transfer in Capillary-Porous Bodies*; Pergamon Press: New York, 1966.
6. Whitaker, S. Coupled transport in multiphase systems. A theory of drying. Advances in Heat Transfer **1998**, *31*, 1–104.
7. Whitaker, S. *The Method of Volume Averaging*; Kluwer Academic: Dordrecht, The Netherlands, 1999.
8. Perre, P.; Turner, I.W. A 3-D version of TransPore: A comprehensive heat and mass transfer computational model for simulation the drying of porous media. International Journal of Heat and Mass Transfer **1999**, *42*, 4501–4521.
9. Blunt, M.J.; Jackson, M.D.; Piri, M.; Valvante, P.H. Detailed physics, predictive capabilities and macroscopic consequences for pore-network models of multiphase flows. Advances in Water Resources **2002**, *25*, 1069–1089.
10. Satik, C.; Yortsos, Y.C. A pore-network study of bubble growth in porous media driven by heat transfer. ASME Journal of Heat Transfer **1996**, *118*, 455–462.
11. Li, X.; Yortsos, Y.C. Visualization and simulation of bubble growth in pore-networks. AIChE Journal **1995**, *41*, 214–222.
12. Dominguez, A.; Bories, S.; Prat, M. Gas cluster growth by solute diffusion in porous media. Experimental and automaton simulation in pore-network. International Journal of Multiphase Flow **2000**, *26*, 1951–1979.
13. Mc Dougal, S.R.; Sorbie, K.S. Estimation of critical gas saturation during pressure depletion in virgin and waterflooded reservoir. Petroleum Geoscience **1999**, *5*, 229–233.
14. Tsimpanogiannis, I.N.; Yortsos, Y.C. The critical gas saturation in a porous medium in the presence of gravity. Journal of Colloid and Interface Science **2004**, *270*, 388–395.
15. Rege, S.D.; Fogler, H.S. Competition among flow, dissolution, and precipitation in porous media. AIChE Journal **1988**, *35*, 1177–1185.

16. Fredd, C.N.; Fogler, H.S. Influence of transport and reaction on wormhole formation in porous media. AIChE Journal **1998**, *44*, 1933–1949.
17. Tsimpanogiannis, I.N.; Lichtner, P.C. Pore-network study of methane hydrate dissociation. Physical Review E **2006**, *74*, 056303.
18. Nowicki, S.C.; Davis, H.T.; Scriven, L.E. Microscopic determination of transport parameters in drying porous media. Drying Technology **1992**, *10*, 925–946.
19. Prat, M. Percolation model of drying under isothermal conditions. International Journal of Multiphase Flow **1993**, *19*, 691–704.
20. Prat, M. Isothermal drying of non-hygroscopic capillary-porous materials as an invasion percolation process. International Journal of Multiphase Flow **1995**, *21*, 875–892.
21. Laurindo, J.B.; Prat, M. Numerical and experimental network study of evaporation in capillary porous media. Phase distributions. Chemical Engineering Science **1996**, *51*, 5171–5185.
22. Laurindo, J.B.; Prat, M. Numerical and experimental network study of evaporation in capillary porous media. Drying rates. Chemical Engineering Science **1998**, *53*, 2257–2269.
23. Prat, M.; Bouleux, F. Drying of capillary porous media with stabilized front in two dimensions. Physical Review E **1999**, *60*, 5647–5656.
24. Le Bray, Y.; Prat, M. Three-dimensional pore-network simulation of drying in capillary porous media. International Journal of Heat Mass Transfer **1999**, *42*, 4207–4224.
25. Yiotis, A.G.; Stubos, A.K.; Boudouvis, A.G.; Yortsos, Y.C. A 2-D pore-network model of the drying of single-component liquids in porous media. Advances in Water Resources **2001**, *24*, 439–460.
26. Huinink, H.P.; Pel, L.; Michels, M.A.J.; Prat, M. Drying processes in the presence of temperature gradients. Pore-scale modeling. European Physical Journal E **2002**, *9*, 487–498.
27. Plourde, F.; Prat, M. Pore-network simulations of drying of capillary porous media. Influence of thermal gradients. International Journal of Heat and Mass Transfer **2003**, *46*, 1293–1307.
28. Yiotis, A.G.; Boudouvis, A.G.; Stubos, A.K.; Tsimpanogiannis, I.N.; Yortsos, Y.C. Effect of liquid films on the isothermal drying of porous media. Physical Review E **2003**, *68*, 037303.
29. Yiotis, A.G.; Boudouvis, A.G.; Stubos, A.K.; Tsimpanogiannis, I.N.; Yortsos, Y.C. The effect of liquid films on the drying of porous media. AIChE Journal **2003**, *50*, 2721–2737.
30. Yiotis, A.G.; Stubos, A.K.; Boudouvis, A.G.; Tsimpanogiannis, I.N.; Yortsos, Y.C. Pore-network modeling of isothermal drying in porous media. Transport in Porous Media **2005**, *58*, 63–86.
31. Segura, L.A.; Toledo, P.G. Pore-level modeling of isothermal drying of pore networks: Effects of gravity and pore shape and size distribution on saturation and transport properties. Chemical Engineering Journal **2005**, *111*, 237–252.
32. Segura, L.A.; Toledo, P.G. Pore-level modeling of isothermal drying of pore-networks accounting for evaporation, viscous flow, and shrinking. Drying Technology **2005**, *23*, 2007–2019.
33. Metzger, T.; Tsotsas, E. Influence of pore size distribution on drying kinetics: A simple capillary model. Drying Technology **2005**, *23*, 1797–1809.
34. Yiotis, A.G.; Tsimpanogiannis, I.N.; Stubos, A.K.; Yortsos, Y.C. Pore-network study of the characteristic periods in the drying of porous materials. Journal of Colloid and Interface Science **2006**, *297*, 738–748.
35. Salin, J.G. Drying of sapwood analyzed as an invasion percolation process. Maderas: Ciencia y Technologia **2006**, *8*, 149–158.
36. Metzger, T.; Tsotsas, M.; Prat, M. Pore-network models: A powerful tool to study drying at the pore level and understand the influence of structure on drying kinetics. In *Modern Drying Technology: Vol. 1. Computational Tools at Different Scales*; Tsotsas, E., Mujumdar, A.S., Eds.; Wiley-VCH: Weinheim, 2007, 57–102.
37. Metzger, T.; Irawan, A.; Tsotsas, E. Influence of pore structure on drying kinetics: A pore network study. AIChE Journal **2007**, *53*, 3029–3041.
38. Metzger, T.; Irawan, A.; Tsotsas, E. Isothermal drying of pore networks: Influence of friction for different pore structures. Drying Technology **2007**, *25*, 49–57.
39. Prat, M. On the influence of pore shape, contact angle and film flows on the drying of capillary porous media. International Journal of Heat Mass Transfer **2007**, *50*, 1455–1468.
40. Segura, L.A. Modeling at pore-scale isothermal drying of porous materials: Liquid and vapor diffusivity. Drying Technology **2007**, *25*, 1677–1686.
41. Yiotis, A.G.; Tsimpanogiannis, I.N.; Stubos, A.K.; Yortsos, Y.C. Coupling between external and internal mass transfer during drying of a porous medium. Water Resources Research **2007**, *43*, 06403.
42. Surasani, V.K.; Metzger, T.; Tsotsas, E. Consideration of heat transfer in pore network modeling of convective drying. International Journal of Heat and Mass Transfer **2008**, *51*, 2506–2518.
43. Shaw, T.M. Drying as an immiscible displacement process with fluid counterflow. Physical Review Letters **1987**, *59*, 1671–1674.
44. Tsimpanogiannis, I.N.; Yortsos, Y.C.; Poulou, S.; Kanellopoulos, N.; Stubos, A.K. Scaling theory of drying in porous media. Physical Review E **1999**, *59*, 4353–4365.
45. Stauffer, D.; Aharony, A. *Introduction to Percolation Theory*; Taylor & Francis: London, 1994.
46. Wilkinson, D.; Willemsen, J.F. Invasion percolation: A new form of percolation theory. Journal of Physics A **1983**, *16*, 3365–3376.
47. Feder, J. *Fractals*; Plenum Press: New York, 1988.
48. Sahimi, M. Flow phenomena in rocks: From continuum models to fractals, percolation, cellular automata, and simulated annealing. Reviews of Modern Physics **1993**, *65*, 1393–1534.
49. Stauffer, D. Scaling theory of percolation clusters. Physics Reports **1979**, *54*, 1–74.
50. Mandelbrot, B.B. *The Fractal Geometry of Nature*; Freeman & Co.: New York, 1982.
51. Birovljev, A.; Furuberg, L.; Feder, J.; Jossang, T.; Maloy, K.J.; Aharony, A. Gravity invasion percolation in two dimensions. Physical Review Letters **1991**, *67*, 584–587.
52. Grossman, T.; Aharony, A. Structure and perimeters of percolation clusters. Journal of Physics A **1986**, *19*, L745–L751.
53. Wilkinson, D. Percolation model of immiscible displacement in the presence of buoyancy forces. Physical Review A **1984**, *30*, 520–531.
54. Wilkinson, D. Percolation effects in immiscible displacement. Physical Review A **1986**, *34*, 1380–1391.
55. Hulin, J.P.; Clement, E.; Baudet, C.; Gouyet, J.F.; Rosso, M. Quantitative analysis of an invading-fluid invasion front under gravity. Physical Review Letters **1988**, *61*, 333–336.
56. Chaouche, M.; Rakotomalala, N.; Salin, D.; Xu, B.; Yortsos, Y.C. Invasion percolation in a hydrostatic or permeability gradient: Experiments and simulations. Physical Review E **1994**, *49*, 4133–4139.
57. Gouyet, J.-F.; Rosso, M.; Sapoval, B. Fractal structure of diffusion and invasion fronts in three dimensional lattices through the gradient percolation approach. Physical Review B **1988**, *37*, 1832–2838.
58. Gouyet, J.-F.; Rosso, M. Diffusion fronts and gradient percolation: A survey. Physica A **2005**, *357*, 86–96.
59. Frette, V.; Feder, J.; Jossang, T.; Meakin, P. Buoyancy-driven fluid migration in porous media. Physical Review Letters **1992**, *68*, 3164–3167.
60. Meakin, P.; Feder, J.; Frette, V.; Jossang, T. Invasion percolation in a destabilizing gradient. Physical Review A **1992**, *46*, 3357–3368.
61. Meakin, P.; Birovlev, A.; Frette, V.; Feder, J.; Jossang, T. Gradient stabilized and destabilized invasion percolation. Physica A **1992**, *191*, 227–239.
62. Meheust, Y.; Lovoll, G.; Maloy, K.J.; Schmittbuhl, J. Interface scaling in a two-dimensional porous medium under combined viscous, gravity and capillary effects. Physical Review E **2002**, *66*, 051603.
63. Chapuis, O.; Prat, M. Influence of wettability conditions on slow evaporation in two-dimensional porous media. Physical Review E **2007**, *75*, 046311.